Informes Técnicos Ciemat **1042**
Mayo, 2004

First Measurements of the Performance of New Semitransparent Amorphous Silicon Sensor Prototypes

CSIC
U. de Cantabria

A. Calderón
E. Calvo
C. Martínez-Rivero
F. Matorras
T. Rodrigo
M. Sobrón
I. Vila
A. L. Virto

CIEMAT

J. Alberdi
P. Arce
J. M. Barcala
A. Fernando
M. I. Josa
J. M. Luque
A. Molinero
J. Navarrete
J. C. Oller
C. Yuste

Departamento de Fusión y Física de Partículas Elementales

Toda correspondenica en relación con este trabajo debe dirigirse al Servicio de Información y Documentación, Centro de Investigaciones Energéticas, Medioambientales y Tecnológicas, Ciudad Universitaria, 28040-MADRID, ESPAÑA.

Las solicitudes de ejemplares deben dirigirse a este mismo Servicio.

Los descriptores se han seleccionado del Thesauro del DOE para describir las materias que contiene este informe con vistas a su recuperación. La catalogación se ha hecho utilizando el documento DOE/TIC-4602 (Rev. 1) Descriptive Cataloguing On-Line, y la clasificación de acuerdo con el documento DOE/TIC.4584-R7 Subject Categories and Scope publicados por el Office of Scientific and Technical Information del Departamento de Energía de los Estdos Unidos.

Depósito Legal: M -14226-1995
ISSN: 1135 - 9420
NIPO: 402-04-005-0

Editorial CIEMAT

CLASIFICACIÓN DOE Y DESCRIPTORES

S44
AMORPHOUS STATE; SILICON; PERFORMANCE; MEASURING METHODS; POSITION SENSITIVE DETECTORS

First Measurements of the Performance of New Semitransparent Amorphous Silicon Sensor Prototypes

Calderón, A.; Calvo, E.; Martínez-Rivero, C.; Matorras, F.; Rodrigo, T.;
Sobrón, M.; Vila, I. and Virto, A.L.
Instituto de Física de Cantabria. CSIC-University of Cantabria* (Santander, Spain)

Alberdi, J.; Arce, P.; Barcala, J.M.; Ferrando, A.; Josa, M.I.; Luque, J.M.;
Molinero, A.; Navarrete, J. and Oller, J.C.

32 pp. 13 figs. 10 refs.

Abstract:

We present first results on the performance of a new generation of semitransparent amorphous silicon position detectors having good properties such as an intrinsic position resolution better than 5 μm, an spatial point reconstruction precision better than 10 μm, deflection angles smaller than 10 μrad and transmission in the visible and NIR higher than 70%. In addition the sensitive area is very large: 30 x 30 cm^2.

Primeras Medidas de las Prestaciones de Prototipos de Nuevos Sensores Semitransparentes de Silicio Amorfo

Calderón, A.; Calvo, E.; Martínez-Rivero, C.; Matorras, F.; Rodrigo, T.;
Sobrón, M.; Vila, I. and Virto, A.L.
Instituto de Física de Cantabria. CSIC-University of Cantabria* (Santander, Spain)

Alberdi, J.; Arce, P.; Barcala, J.M.; Ferrando, A.; Josa, M.I.; Luque, J.M.;
Molinero, A.; Navarrete, J. and Oller, J.C.
CIEMAT** (Madrid, Spain)

32 pp. 13 figs. 10 refs.

Resumen.

Presentamos primeros resultados sobre las prestaciones de una nueva generación de detectores de posición semitransparentes, de silicio amorfo, que presentan propiedades tales como una resolución intrínseca mejor que 5 μm, una precisión de reconstrucción espacial mejor que 10 μm, unos ángulos de deflexión inferiores a 10 μrad y un poder de transmisión en el visible y el NIR mayor que el 70%. Además disponen de un área sensible muy grande: 30 x 30 cm^2.

---

* Under CICYT (Spain) grant AEN 99-0571.
** Under CICYT (Spain) grant aen 99-0312.

1. Introduction

In some applications, as for example the precise multipoint alignment, one needs to measure and/or monitor accurately (few μm) the space position of a laser beam at several points along its light path. In such cases the simplest solution is to use transparent position sensors. When the expected independent motions of the pieces are big (i.e. from mm to a couple of cm) the active area of the sensors should be large. In this work we will present first results on the characterization of a new generation of semitransparent amorphous silicon 2D position detecting sensors for multipoint alignment (ALMY) that, in addition to a very acceptable performance, have the largest active area ever constructed: 30 x 30 mm^2.

In general, ALMY [1] sensors are semitransparent two dimensional position strip sensors. They are built on top of a glass substrate and use amorphous silicon as photoactive material, which, for very thin layers, has the property of being almost transparent for visible light. The amorphous silicon is deposited between two layers of perpendicular strips electrodes.

Each volume of a-Si:H enclosed in the intersection of one upper and one bottom electrodes defines a Schottky photodiode. The position of a light spot on the sensor surface is determined as the centre of gravity of the photocharge distribution collected by the 2D grid of photodiodes.

The way of accessing the photodiodes in the ALMY is a characteristic of the sensor: if $N_{x(y)}$ is the number of photodiodes along the two orthogonal coordinates X (Y), the ALMY sensor contains $N_x \times N_y$ photodiodes but they are accessed as a set of $N_x + N_y$ rows and columns of photodiodes.

Amorphous silicon can work in very extreme radiation environments [2] and it is not affected by intense magnetic fields because of its low Hall mobility and small drift length of carriers.

ALMY sensors were first developed by Kroha et al. [1] at the Max Planck Institute and after commercialised by EG&G [3].

Commercial ALMYs were studied by us time ago [4]. The measured precision on spot reconstruction was about 5 μm. However, the transmittance in the visible was lower than 50%, unabling the installation of a large number of sensors on the same light path. Moreover, the measured deflections of the laser beam when crossing a single sensor were found to be very large: above 50 μrad with dispersions (the rms of the angular distributions) even larger. That unables the possibility of offline corrections. In addition, and for some applications, the active area available was insufficient.

We present, in this document, first measurements on the performance of five prototypes of a new generation of ALMY sensors having a large active area, developed by M. Schubert and his group at the Silicium Department of the *Institut für Physikalische Electronik* (Stuttgart University)[5].

The document is organized as follows: General sensors specifications, readout and control are given in section 2, signal reconstruction and position reconstruction intrinsic resolution are presented in section 3. Section 4 deals with the determination of the sensitivity, uniformity of the response and black current, while linearity measurements and the calculation of the light spot spatial reconstruction precision are explained in section 5. Beam transmission studies such as measurement of deflection angles and transmittance spectra are given in sections 6 and 7, respectively. Section 8 is devoted to ageing studies

and section 9 to the consequences of the gamma-ray irradiation on the sensors performance. Finally we draw some conclusions in section 10.

2. General ALMY sensors specifications, readout and control

The new generation of ALMY sensors are constructed following the sketch in Fig. 1. They consist of a layer of hydrogenated amorphous silicon (a-Si:H) of ~ 300 nm thickness sandwiched between two layers of ~ 100 nm zinc oxide (ZnO) electrodes perpendicularly segmented to draw a 2D semitransparent matrix of 64 x 64 Schotky photodiodes.

The zinc oxide is segmented using photolithographic methods. The three layers are deposited onto a ~ 1 mm thick glass substrate. The glass is coated with an antireflection treatment which should minimize interferences and reduce deflection angles [4].

Laser light is partially absorbed by the a-Si material producing photocurrents on the strips. Saturation occurs at about 3.7 μA (1000 ADC counts). The signal, extracted via ZnO:Al pads, is multiplexed, converted to voltage and transferred to the ADC of the microcontroller. The most important parameters of these sensors are summarized in Table 1.

The strips layout allows to have two orthogonal projections of the incoming beam. Vertical strips reproduce the projection of the beam spot along X while horizontal strips do the same along Y.

The electronic addresses each sensor and sends the data to a PC. Raw data are transmitted to the PC through the serial RS232 port and the readout is controlled by a dedicated driver programmed with LabView [6].

3. Signal reconstruction, stability and intrinsic position resolution

3.1 Experimental set-up

The experimental set-up for stability tests and determination of the intrinsic position resolution consisted of a laser working in the visible light range (633 nm He-Ne), optical filters, and the ALMY under test, located about 5 m downstream the laser source. Both elements were placed on a granite optical bench.

3.2 Signal reconstruction

Due to the geometry of the ALMY electrodes, information about the incoming beam is obtained in the form of two orthogonal intensity profiles. The X and Y projections of the light distribution are fitted to Gauss Ian functions and their mean values determine the position of the centre of the light spot on the ALMY active area.

3.3 Stability tests and intrinsic position resolution

We made short stability tests using ALMY units A1 and A2. Data were taken with the light beam always pointing (within the laser stability) to the same place of the active area. In each test we have taken 100 data points, lasting in total about 20 min.

As an example, Figs. 2 a) and b) show the distribution of the reconstructed spot centre (both coordinates), in ALMY unit A1. The width of the distributions will be taken as the

device intrinsic position resolution. They are σ_x = 1.7 μm and σ_y = 2.7 μm in the X and Y coordinates, respectively. Results for unit A2 are σ_x = 1.5 μm and σ_y = 2.0 μm.

Notice that measured resolutions are upper values because they are of the same order than the laser stability. From a previous work, using extremely precise crystal silicon pixel matrix detectors [7], it can be extracted that the outgoing light beam from the head of the used He-Ne unit is moving, in a Gaussian-like way, inside a cone of about 0.4 μrad opening angle. At 5 m distance that means an average deviation of about ± 1 μm from the axis of the light exiting cone.

4. Sensitivity and uniformity of the response

4.1 Experimental set-up

To study the diode-to-diode variation response to a uniform illumination, a white light from a halogen lamp mounted in the focus of a dichroic reflector and coupled to a diffuser illuminated the whole sensor sensitive area. The distance diffuser ALMY was about 1.5 m. The irradiance of the lamp was controlled with a crystal silicon photovoltaic cell. The cell was previously calibrated to convert output current (mA) to irradiance (mW/cm^2).

Of course, when reading the current from one strip, one is reading the current from 64 diodes. We have, in the analysis, made the assumption that all diodes in a given strip are giving the same response.

In addition, we have observed in the prototypes some defects inherent to a first production: some strips fail in connection and give either no current or saturate or show unphysical response. All diodes belonging to such strips are not considered in the calculations.

4.2 Uniformity of the photoresponse

Units A1, A3 and A4 were exposed, in turn, to a uniform light of irradiance E = 1.32 mW/cm^2. As an illustration, we show in Fig. 3 a plot of the diodes response (in mA/W) of sensor A3 as a function of their position on the ALMY surface. Apart from non working strips, the figure presents a quite uniform pattern.

To quantify sensitivity and uniformity we show in Fig. 4 the distribution of the diodes response corresponding to sensor A3. The mean value is 17.1 mA/W with an rms of 0.3 mA/W. Table 2 summarizes the results for the 3 studied units. Mean values for diode response are very similar in all the three sensors and all of them show a diode-to-diode uniformity (3σ) in the response better than 6%.

4.3 Dark current measurement

We have measured in two of the units the diodes currents in obscurity. Figs 5 a) and b) show the distribution of the diode current for sensors A3 and A4, respectively. Distributions are quite narrow. The resulting average dark current per diode is 0.4 ± 0.1 nA in sensor A3 and 0.6 ± 0.1 nA in sensor A4. The errors are the rms of the corresponding distributions.

5. Linearity and spatial reconstruction precision

Linearity measurements indicate how well the sensor reconstructs displacements of the light spot. It allows to determine the minimum displacement the sensor can resolve.

5.1 Experimental set-up

The ALMY under test is placed on two motorized platforms, 2 μm resolution each, 0.5 m downstream a laser source. The platforms allow performing horizontal (along the X coordinate) and vertical (along the Y coordinate) scans over a 20×20 mm^2 surface of the sensor.

During horizontal scans light collected in the vertical strips allows to reconstruct the horizontal displacement of the light spot. The same argument stands for a vertical scan and horizontal strips.

The operation is done as follows: starting from an arbitrary initial position, the sensor is scanned, by moving the platforms, in steps of about 1 mm in both directions, to cover the accessible surface. At every point of the scan, data are taken and the centre of the light spot is reconstructed and recorded. A matrix of 20×20 points is obtained in this way.

The beam position, reconstructed on the sensor is expected to have a linear dependence on the real displacement of the moving platform.

The departure from the linear behaviour, evaluated as the width (rms) of the residuals with respect to a linear fit, defines the spatial point reconstruction precision (in both X and Y coordinates) of the sensor.

Measurements were done for ALMY unit A1 in obscurity conditions. A He-Ne light source was used.

5.2 Results

Every 2D scan is analyzed independently either as 20 one-dimensional scans along X or as 20 one dimensional scans along Y, for a fixed position of the orthogonal co-ordinate. As an example, Fig. 6 shows the reconstructed beam position on the sensor, as a function of the real displacement along the Y direction for a single scan (i.e. one particular column of the 20×20 matrix). Data points were fitted to a linear function. The fitted slope is 1.01 ± 0.01. The corresponding residuals to the linear fit, as a function of the Y position, are shown in the small drawing inside Fig. 6. Their distribution, centred at zero, has an rms of 9.8 μm.

Figs. 7 a) and b) show the distribution of the residuals in the X and the Y directions, respectively, for the whole scan of sensor A1. The distributions are well centred at zero. Their widths give the spatial point reconstruction precision in the X and the Y directions. For this sensor, $\sigma_x = 9.9$ μm and $\sigma_y = 6.2$ μm.

5.3 Discussion

The measured space point reconstruction precision is less than 10 μm, which is a very acceptable value, in both directions. However the distributions shown in Fig. 7 have long tails.

When inspecting the uniformity of the photoresponse of the various sensors, we have noticed defects in the prototypes that lead to non usable strips (see Fig. 3) due to construction errors arising from various sources.

When scanning the sensor, the light spot crosses, at some places of the active area, one or more bad strips which results in a poor reconstruction of the center of the spot and, therefore, leading to a bad linear fit. The full distribution of the residuals become large and have tails of non negligible values corresponding to the badly reconstructed points.

Extreme values of the residuals in the distribution in Fig. 7 a) are –54.1 and 25.5 μm, while in Fig. 7 b) are –15.9 and 18.8 μm.

6. Beam deflections

Light propagating through a medium suffers interactions with the matter and thus changes its speed and propagation direction. Moreover, when light traverses several layers of materials, part of the incoming energy is reflected in the interfaces of the media. and interferences may appear due to the phase difference between incoming and reflected light. The combination of these effects are at the origin of beam deflections: the outgoing ray emerges in a different direction with respect to the incoming ray.

To minimize interference effects, the glass substrate of the studied prototypes is treated with an antireflection coating, the thickness is just one millimetre and its plan parallelism is better than 5 μm, with a very good flatness. In addition, electrode and silicon layers are extremely thin.

The deflection angle was measured for some prototypes to evaluate the effectiveness of the construction procedure.

6.1 Experimental set-up

The experimental set-up (see sketch in Fig. 8) consisted in a monomode laser source (we used sources of two wavelengths, a He-Ne and a 785 nm diode), a first ALMY located at ~0.5 m from the light source and installed on two motorized platforms and a second ALMY, installed several meters downstream (~ 5 m) from the first one, in a fixed position. All components are placed on a stable granite optical bench.

The measurement of the deflection angles (Θ_x and Θ_y) is done studying the reconstructed signal on the second sensor while scanning the sensor under test. First, the second sensor records the undeflected beam when the first one is removed from the light path. This position is used as reference. The reconstructed beam position when the first sensor is back in the light path is then compared with the reference. The angle definition is sketched in Figure 9.

6.2 Results

The deflection angles were measured for sensors A1 and A2, using two different laser sources and found mean values and dispersions below 10 μrad for both Θ_x and Θ_y angles, as shown in Table 3. The errors are the rms of the corresponding distributions. The total deflection angle (see Fig. 9) is defined as $\Theta = \sqrt{(\Theta_x^2 + \Theta_y^2)}$.

7. Transmittance

The transmittance is the percentage of the transmitted light through a sensor. It has been measured using an spectrophotometer.

7.1 Results

We have measured the transmittance to four of the prototypes in the UV, visible and the IR regions. They all have a transmission power higher than 70% in the full visible range and in the NIR region. Table 4 displays the values found for some wave-lengths. Measurement errors are of the order of 1 %.

8. Ageing

It is known that properties of a-Si:H are susceptible to change upon prolonged illumination. This is known as the Staebler and Wronsky Effect (SWE) [8], also called ageing phenomena.

To measure the degradation of the response and how this affects the overall performance, we have exposed unit A2 to a prolonged illumination.

8.1 Experimental set-up

The experimental set-up consisted of a 670 nm laser diode, coupled to a monomode fibre, some optical filters, a beam splitter and the sensor under test, installed on the motorized platforms.

The laser beam is partially deflected (2.7%) at the splitter in order to monitor the laser power all along the experiment.

Light spot at the sensor surface had 3 mm diameter, with an average irradiance of 7.9 mW/cm^2. The laser beam affects a square of about 8x8 photodiodes (ageing place). The A2 sensor was exposed for a total of 715 hours.

8.2 Measurements and results

Along the time of exposition, we have made some measurements in 15 occasions. The measurements consisted of a readout of the current induced by the light spot on the sensor, a reconstruction of the centre of gravity of the spot and a scan (using the motorized platforms where the sensor in test is placed) of the active area around the ageing place. Once the scan is finished the motorized platforms place back the sensor such as the laser points again to the ageing area and the exposition continues.

The output current from the ageing area, as a function of the illumination time, can be seen in Fig. 10. The sensor loses sensitivity very fast along the first 70 hours of illumination, presenting a degradation of about 30% with respect to t = 0. Afterwards sensitivity degrades almost linearly with the illumination time with a slope of about -0.03%/h. By the end of the ageing exposition, t = 715 h, the sensitivity of the sensor was reduced to 54% of the initial one. This loss of sensitivity is affecting, as we will see, the resolution of the spatial reconstruction of the centre of the light spot.

The sensor is scanned in an area of 6 × 6 mm^2, cantered in the exposed region. It is scanned along 12 horizontal lines, with 10 points per line. Spatial separation between two consecutive points of the scan is ~ 500 μm in both directions. The first two and the last two lines in the scan (labeled 1, 2, 11 and 12) run out of the ageing area. On the contrary, lines 5 to 8 will cross the ageing place. "Non affected lines" are used as control for comparisons.

The aim of this search is to have an estimation about the lose of linearity, and therefore, of precision in the space point reconstruction, due to the ageing phenomena. As in section 5, a linear fit is performed to the reconstructed position as a function of the motor position. This is done for the 12 lines in observation. As seen earlier, in the absence of ageing, the fitted slope should be essentially 1 for all the lines.

Fig. 11 shows the fitted slopes for the scanning of lines 1 (diamonds), 6 (dots) and 7 (circles), respectively, as a function of the illumination time. The slope for strip 1 stays fairly constant and equal to 1.01, while those for strips 6 and 7 increase with the elapsed illumination time.

The effect of the ageing on the spatial point reconstruction precision can be extracted from the above linearity measurements. We present in Fig. 12 the width of the distributions of the residuals from the linear fits, as a function of the elapsed illumination time, for the scanning over lines 1 (dots) and 6 (circles). The spatial precision degrades from about 5 μm to more than 20 μm.

9. Transmittance and gamma-ray irradiation

The primary effect induced by photon radiation on transparent materials is a reduction of the light transmission (browning): in glasses, for instance, radiation causes the formation of color centres via the creation of defects in the lattice structure [9]. There may also be changes in the properties of the layers conforming the sensor: refraction index, chemical composition or even thickness. All these changes may cause a variation in the original light transmission spectrum.

We have therefore investigated the eventual effect of the gamma-ray irradiation in the transmission using one of the sensors in test (sensor A5). The sensor was irradiated up to 100 kGy (Si) in two steps of 50 kGy each. The transmittance was measured before and after every irradiation step.

The gamma irradiation was done at the NAYADE [10] facility (a water pool) of CIEMAT, Madrid. We used, in both irradiation steps, ^{60}Co sources delivering a total flux about 1 kGy(Si)/hour. The irradiation was done at about 15.5 °C. Error in the delivered dose is 8 %.

Transmission was measured with a spectrophotometer. Results are shown in Fig. 13. White triangles correspond to the measurements done before irradiation. Black triangles represent the results after the first 50 kGy and white circles correspond to the measured

transmission after a total ionisation dose of 100 kGy. A summary of numerical results for some wavelengths are given in Table 5.

As one can see, the range 650 nm – 800 nm is affected, after the first 50 kGy irradiation dose, by a slight reduction in the transmittance of about 5 – 10 %. After the second 50 kGy dose, the transmission spectrum appears significantly different from the original one. In the visible, the loss of transmittance may exceed 20% and in the NIR a maximum in the transmittance appears where there was a minimum. For instance (see Table 5), for the (900 ± 5) nm range, we measured (75.0 ± 0.1) % before irradiation and (83.2 ± 0.7) % after 100 kGy.

Reasons for such a change in the NIR have been already mentioned. One interpretation is that the observed changes reflects the change in the interference diagrams because radiation induced variations in the refraction index and/or in the thickness of the various layers. It may also have happened that the zinc oxide electrodes have suffered a reduction process and the ratio ZnO/Zn metallic has decreased. In such case, one would expect an increase in the absorption in the IR and therefore a decrease of the transmission in that wavelength range. The measurements stop at 1100 nm and therefore we do not know what happens in the IR, but the observed change of the curvature in the NIR (see Fig. 13) may be an indication of such effect.

10 Conclusions

First measurements of a few prototype units of the new large area semitransparent amorphous silicon sensors manufactured by M. Schubert and his Group at the Silicium Department of the *Institut für Physikalische Electronik* (Stuttgart University)[5], allow to draw the following conclusions on their performance:

- The investigation of the electrical characteristics of the prototypes reveals some construction faults that have to be corrected, such as non connected strips, short cuts and interconnection of adjacent electrodes, defects all of them giving rise to non usable strips.
- Measured intrinsic position resolution is better than 3 μm in both X and Y directions.
- The average response per photodiode is very good: about 10 mA/W. The non uniformity of the response over the full active area is low and of the order of 6%. The measured dark current is more than two orders of magnitude smaller than the signal.
- The spatial point reconstruction precision is measured to be better than 10 μm in both X and Y directions.
- Deflection angles result to be small (< 10 μrad) and present narrow distributions (rms smaller than 10 μrad).
- Transmission power is higher than 70% for the full visible range and the NIR, that makes these sensors very appropriate for multipoint alignment purposes.
- Measured ageing effects are similar to those found in silicon detectors by other authors.
- Gamma-ray irradiation below 50 kGy (Si) will not cause any significant change in performance.

References

[1] W. Blum, H. Kroha and P. Widmann, Nucl. Instr. Meth. A367 (1995) 413.
[2] M. Yamaguchi, S.J. Taylor, S. Matsuda & O. Kawasaki, Applied Physics Letters, 68. (1996) 3141-3143.
[3] EG&G Optoelectronics, 45 William Street, Wellesley, MA02181, USA.
[4] M.G. Fernández, et al., Nucl. Instr. Meth. A440 (2000) 372.
[5]http://www.ipe.uni-stuttgart.de
[6] LabView, National Instruments Corporation, 6504 Bridge Point Parkway Austin, TX 78730-5039,USA.
[7] A.L. Virto et al., Nucl. Instr. Meth. A497 (2003) 397.
[8] D.L. Staebler and C.R. Wronsky, Appl. Phys. Lett. 31 (1977) 292.
[9] L. Patter, Hardening assurance and qualification of components and systems, Tutorial Short Course, Section IV, RADECS 99 Conference, pp. 1-40.
[10] Nayade Irradiation Facility (http://www.ciemat.es/eng/instalacion/0i070.html)

Table Captions

Table 1: Geometry of the new transparent position detectors.
Table 2: Measured photoresponse (see text).
Table 3: Results from deflection measurements (see text).
Table 4: Transmission measurements (in %) at different wavelengths in 4 sensors.
Table 5: Transmission measurements (in %) at some wavelengths before and after gamma-irradiation periods.

a-Si:H thickness	300 nm
Strip thicknes	100 nm
Glass thicknes	1 mm
Active area	30 mm x 30 mm
Number of strips	64 horizontal + 64 vertical
Strip pitch	430 μm
Strip gap	22 μm

Table 1: Geometry of the new transparent position detectors

Sensor	<diode response (mA/W)>	rms (mA/W)
A1	17.8	0.3
A3	17.1	0.3
A4	17.5	0.3

Table 2: Measured photoresponse (see text)

Sensor label	laser	Wavelength (nm)	Θ_x (μrad)	Θ_y (μrad)	Θ (μrad)
A1	diode	785	-1.7 ± 2.9	3.0 ± 3.5	5.1 ± 2.5
A2	diode	785	1.0 ± 2.6	-1.6 ± 2.8	4.2 ± 2.3
A1	He-Ne	633	-1.0 ± 4.4	2.0 ± 3.5	5.1 ± 3.2
A2	He-Ne	633	-0.6 ± 1.9	-1.6 ± 2.3	3.1 ± 1.5

Table 3: Results from deflection measurements (see text).

Sensor label	633 nm	670 nm	785 nm	900 nm	1000 nm
A1	78	86	88	72	88
A2	76	81	89	75	87
A3	74	79	87	74	85
A4	77	82	90	75	86

Table 4: Transmission measurements (in %) at different wavelengths in 4 sensors

Total Ionization Dose(kGy)	(500±5)nm	(600±5)nm	(700±5)nm	(800±5)nm	(900±5)nm	(1000±5)nm
0	2.3 ± 0.4	46.4 ± 3.5	86.2 ± 0.5	87.7 ± 0.5	75.0 ± 0.1	87.2 ± 0.1
50	1.8 ± 0.3	37.0 ± 3.0	76.8 ± 0.8	85.6 ± 0.3	76.8 ± 0.1	84.5 ± 0.1
100	2.3 ± 0.4	31.1 ± 1.5	64.3 ± 0.1	71.9 ± 0.3	83.2 ± 0.7	77.2 ± 0.9

Table 5: Transmission measurements (in %) at some wavelengths before and after gamma-irradiation periods

Figure Captions

Fig.1: Sketch of the sensor showing the layer arrangement. The drawing is not scaled.

Fig. 2: Data from one stability test. Reconstruction of the laser spot center:

a) X coordinate,
b) Y coordinate.

Fig. 3: Response of ALMY A3 diodes to a uniform white light as a function of their location in the sensor.

Fig. 4: Distribution of the diodes response of the ALMY A3 sensor to uniform light.

Fig. 5: Distribution of the diode current in obscurity for sensors: a) A3 and b) A4.

Fig. 6: Linearity test of sensor A1: reconstructed Y position versus real Y position for a single scan. Data points are fitted to a straight line. The residuals with respect to the fit, as a function of the real Y position, can be seen in the inner figure.

Fig. 7: Linearity test from the full scan of sensor A1:

a) Distribution of the X residuals,
b) Distribution of the Y residuals.

Fig. 8: Sketch of the deflection angles measurement experimental set-up.

Fig. 9: Sketch of the deflection angles definition. For simplicity only the total deflection angle is represented.

Fig. 10: Sensor output current (arbitrary units) as a function of the elapsed illumination time.

Fig. 11: Linearity constants from the scan along lines 1 (dots) and 6 (circles), as a function of illumination time (see text).

Fig. 12: From linear fits (see text): widths of the residual distributions as a function of the elapsed illumination time for lines 1 (dots) and 6 (circles).

Fig. 13: Measured transmittance as a function of the wavelength before irradiation (white triangles), after 50 kGy(Si) (black triangles) and after a total accumulated dose of 100 kGy(Si) (white circles) of gamma-ray irradiation.

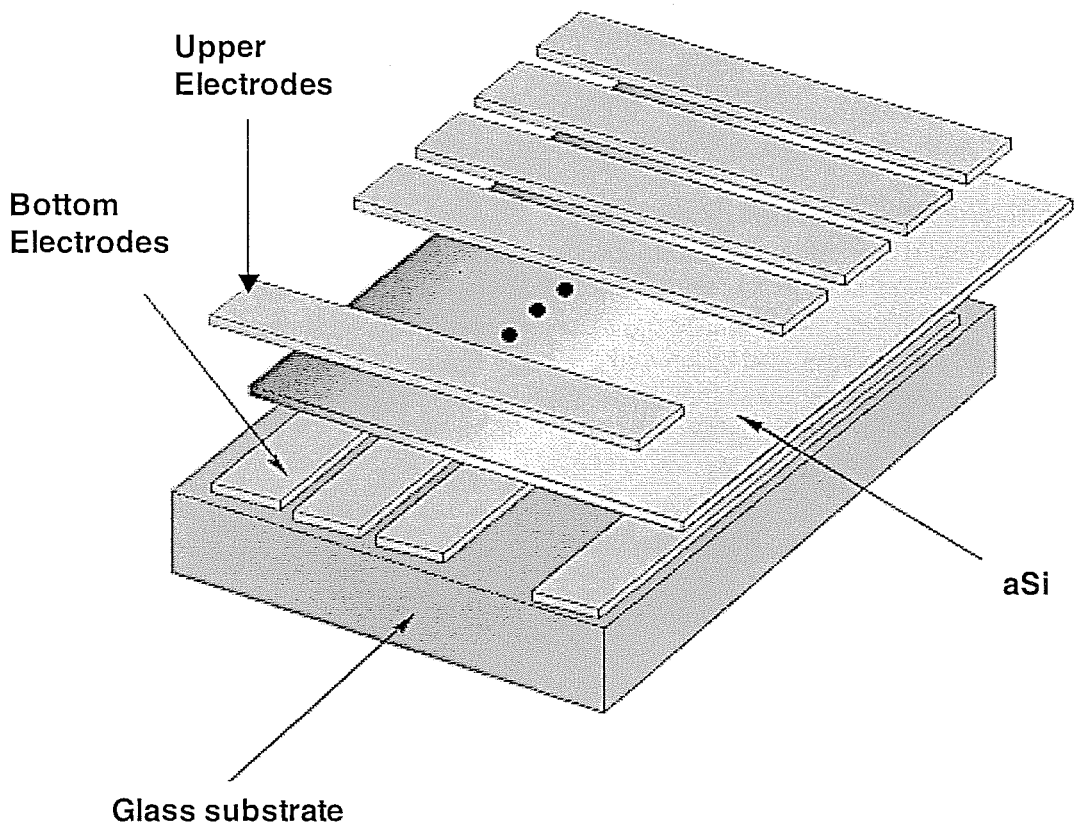

Fig. 1

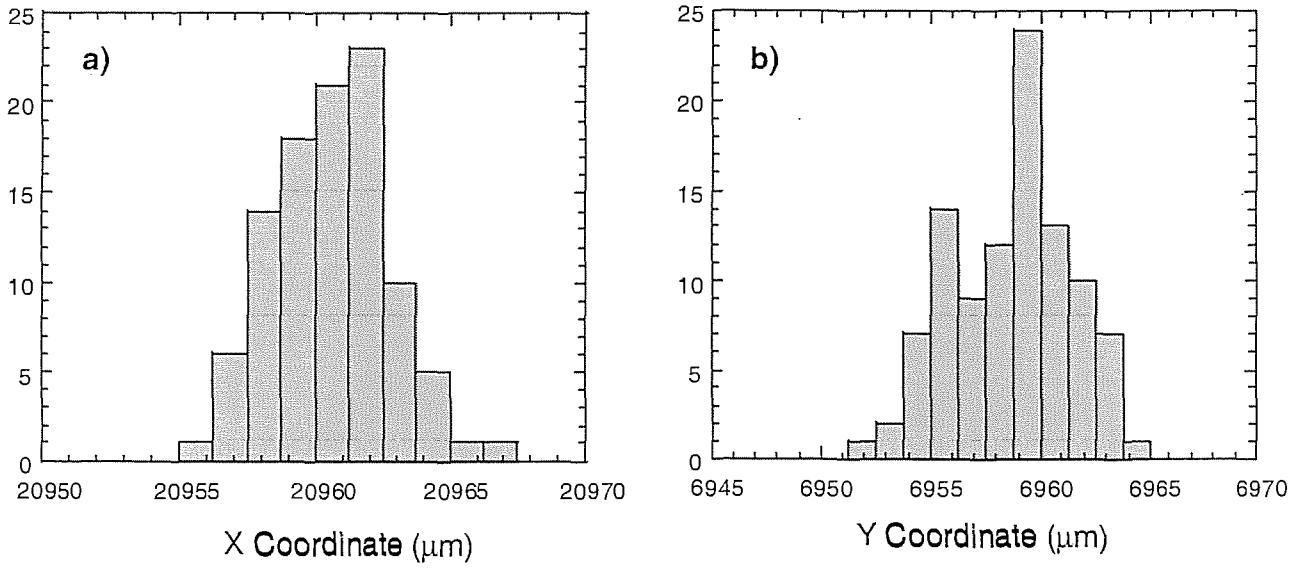
a)
25
20
15
10
5
0
20950
20955
20960
20965
20970
X Coordinate (μm)
b)
25
20
15
10
5
0
6945
6950
6955
6960
6965
6970
Y Coordinate (μm)

Fig. 2

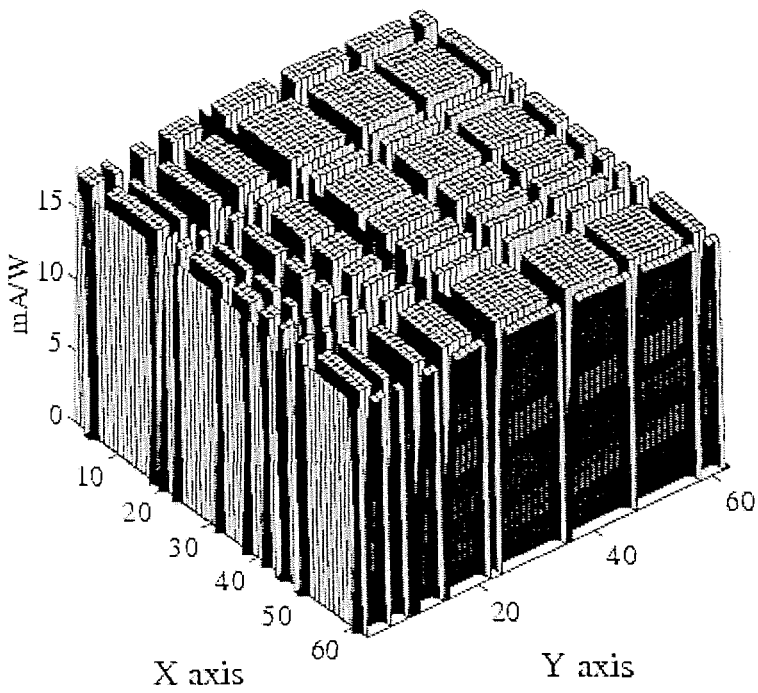

Fig. 3

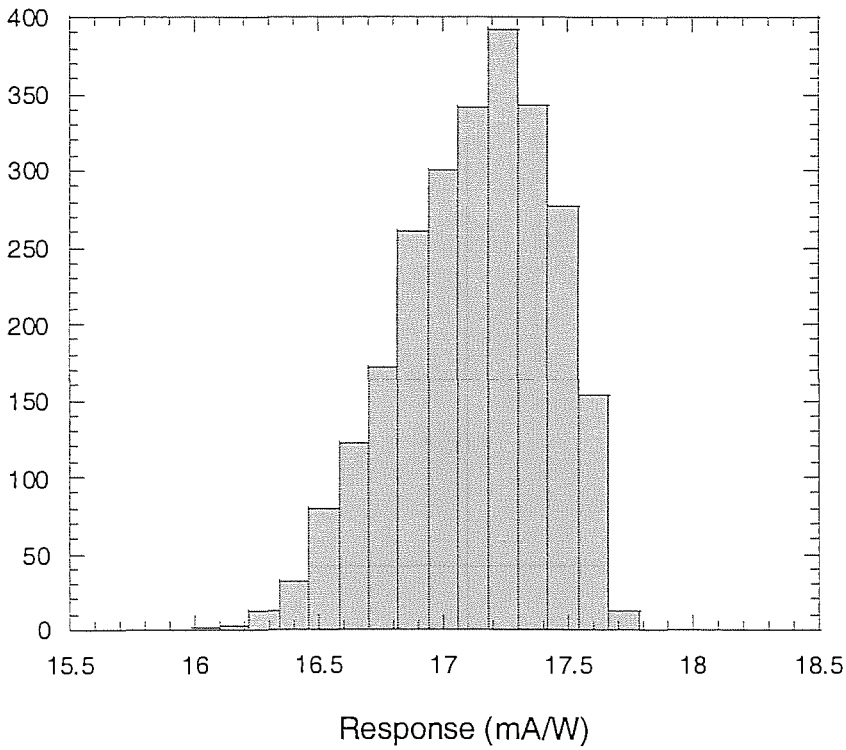
400
350
300
250
200
150
100
50
0
15.5
16
16.5
17
17.5
18
18.5
Response (mA/W)

Fig. 4

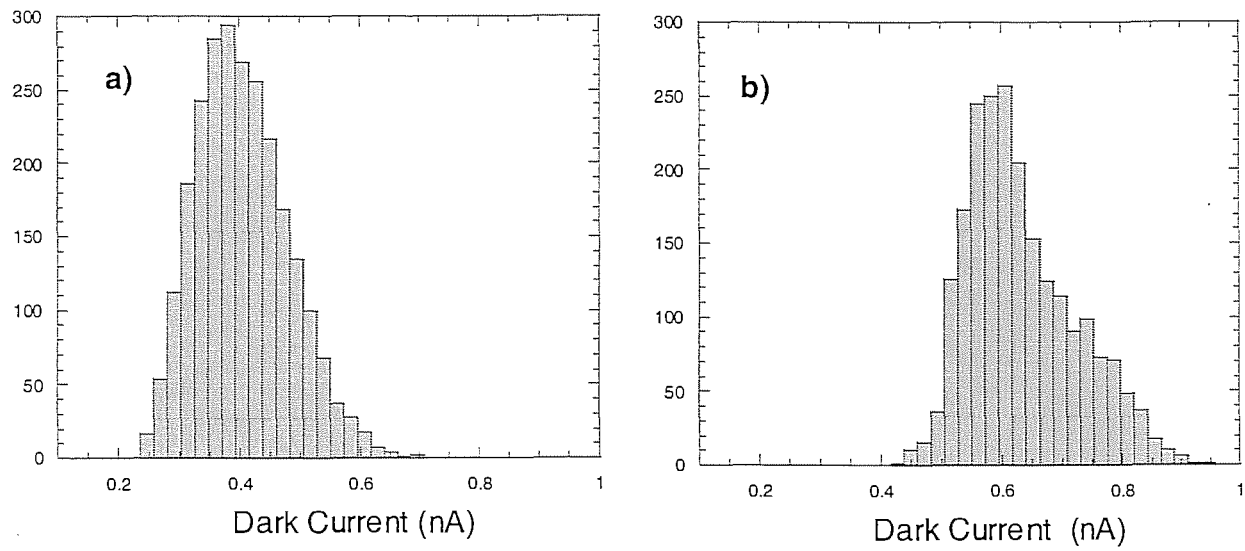
a)
b)
300
250
200
150
100
50
0
0.2
0.4
0.6
0.8
1
Dark Current (nA)
Dark Current (nA)

Fig. 5

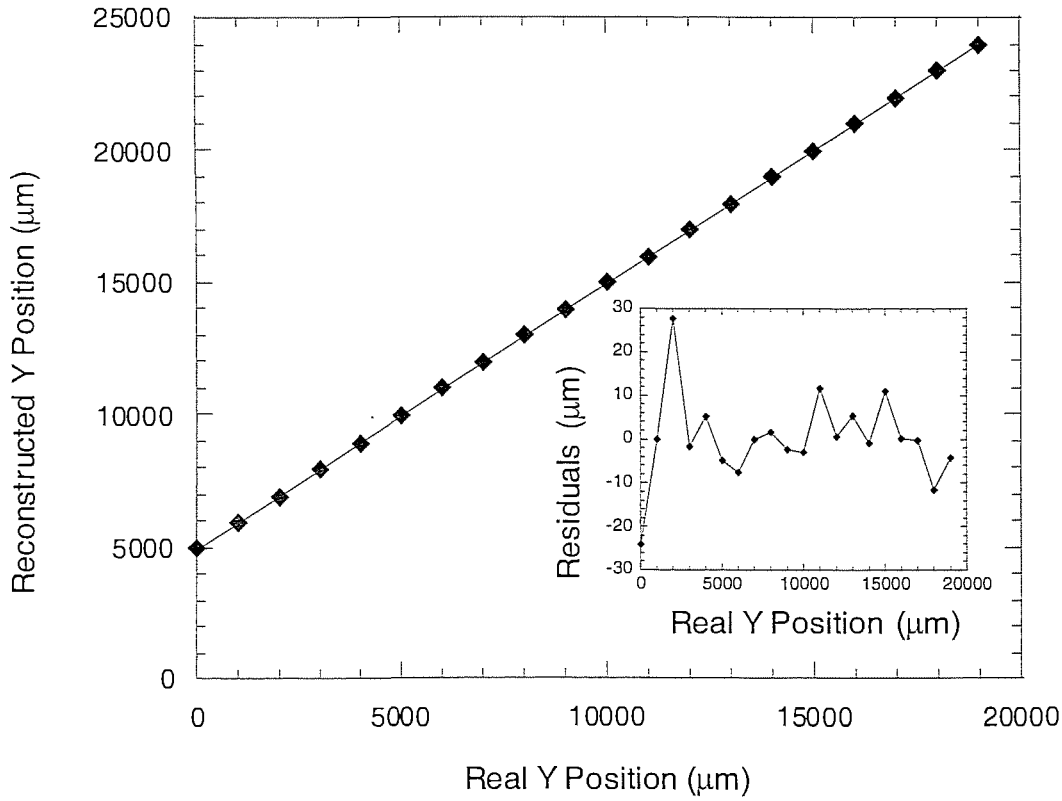
25000
20000
15000
10000
5000
0
Reconstructed Y Position (μm)
0
5000
10000
15000
20000
Real Y Position (μm)
Residuals (μm)
30
20
10
0
-10
-20
-30
0
5000
10000
15000
20000
Real Y Position (μm)

Fig. 6

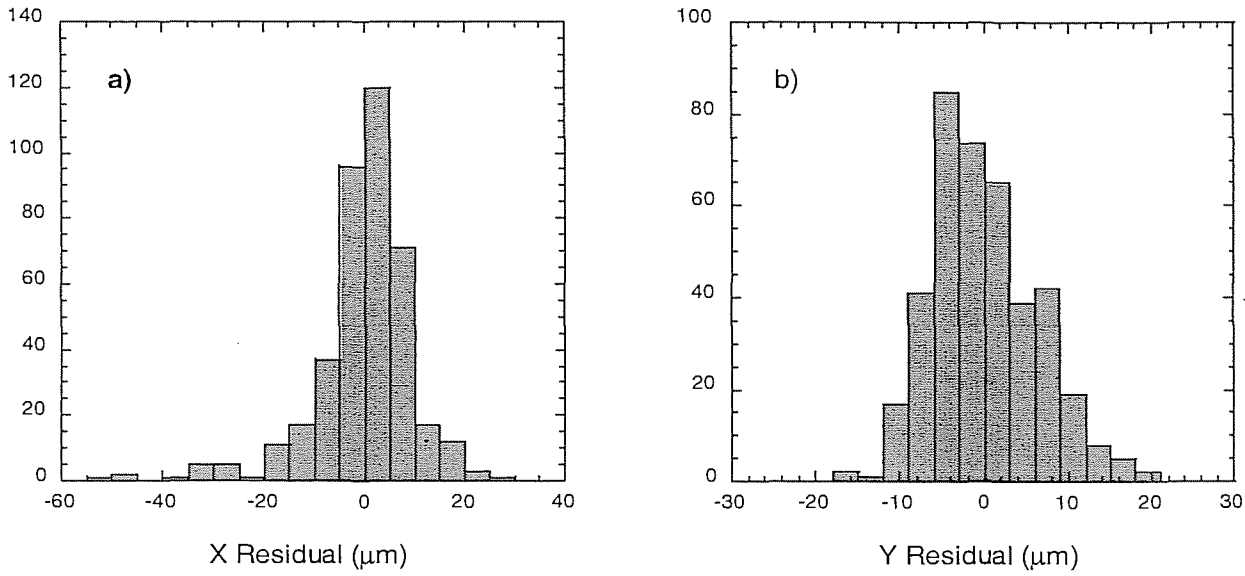
a)
140
120
100
80
60
40
20
0
-60
-40
-20
0
20
40
X Residual (μm)
b)
100
80
60
40
20
0
-30
-20
-10
0
10
20
30
Y Residual (μm)

Fig. 7

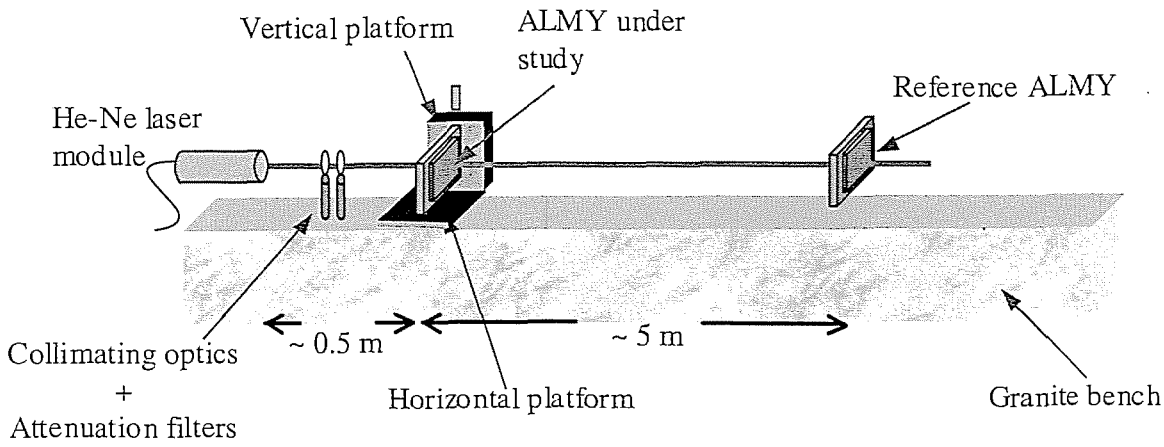
Vertical platform
ALMY under study
Reference ALMY
He-Ne laser module
Collimating optics + Attenuation filters
~ 0.5 m
~ 5 m
Horizontal platform
Granite bench

Fig. 8

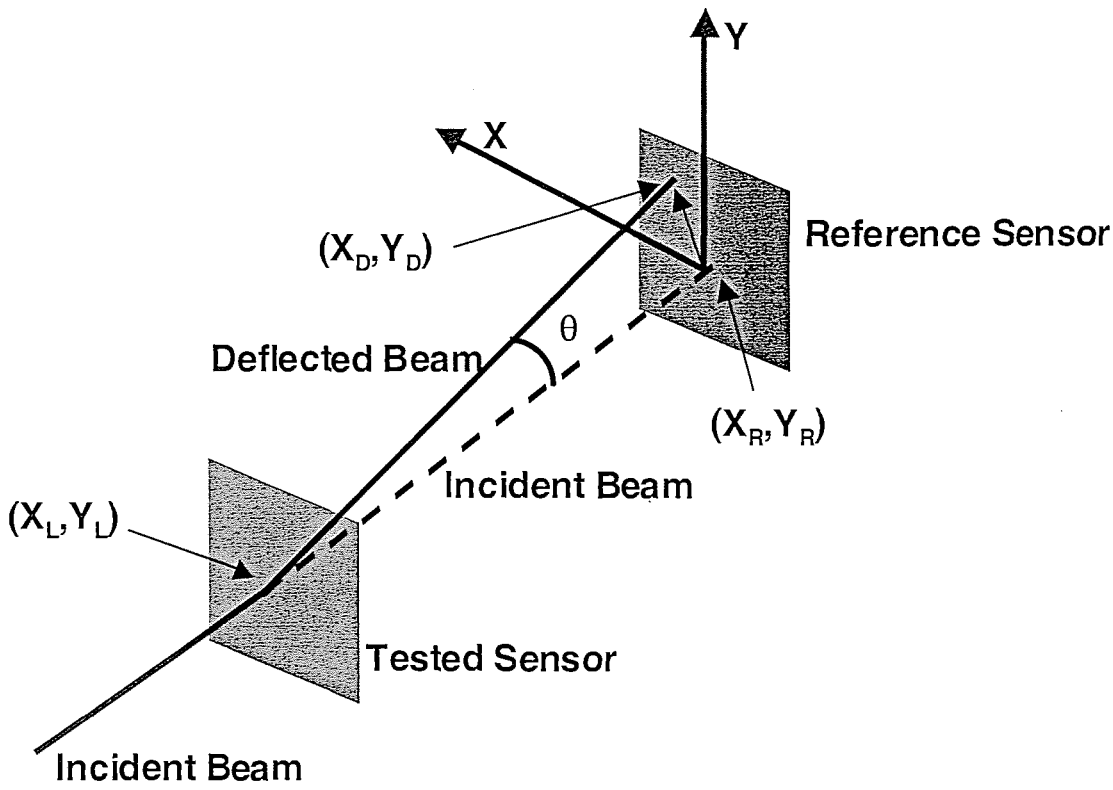
Y
X
(X_D, Y_D)
Reference Sensor
Deflected Beam
θ
(X_R, Y_R)
Incident Beam
(X_L, Y_L)
Tested Sensor
Incident Beam

Fig. 9

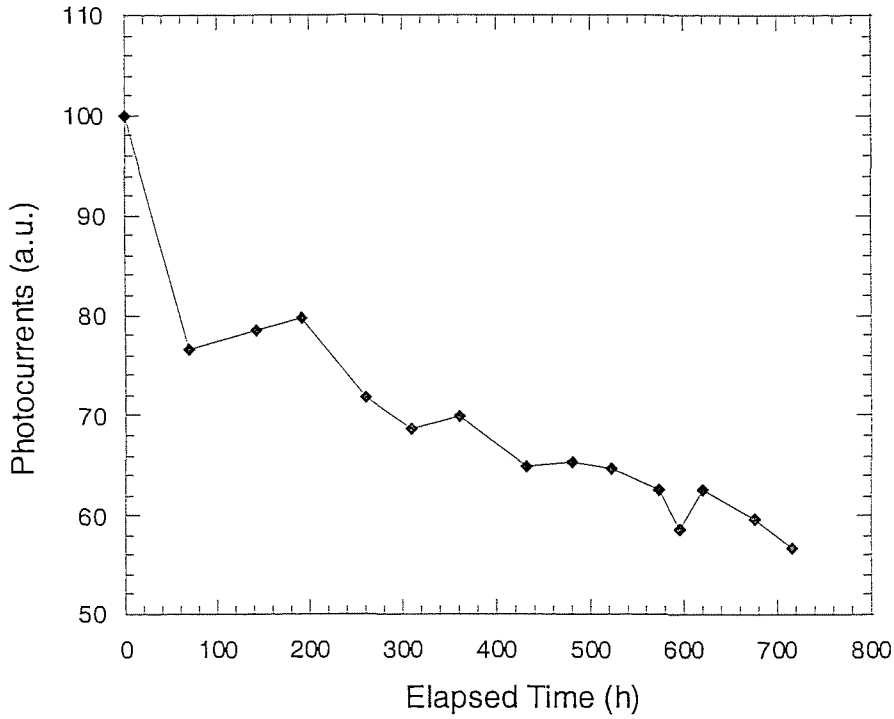
110
100
90
80
70
60
50
Photocurrents (a.u.)
0
100
200
300
400
500
600
700
800
Elapsed Time (h)

Fig. 10

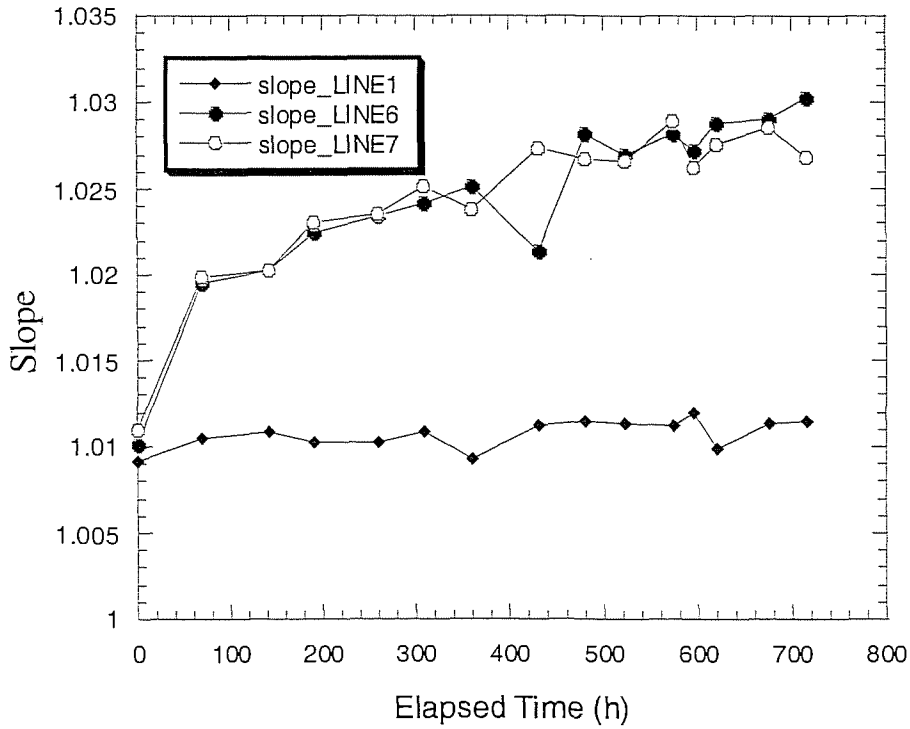
slope_LINE1
slope_LINE6
slope_LINE7
Slope
Elapsed Time (h)
1.035
1.03
1.025
1.02
1.015
1.01
1.005
1
0
100
200
300
400
500
600
700
800

Fig. 11

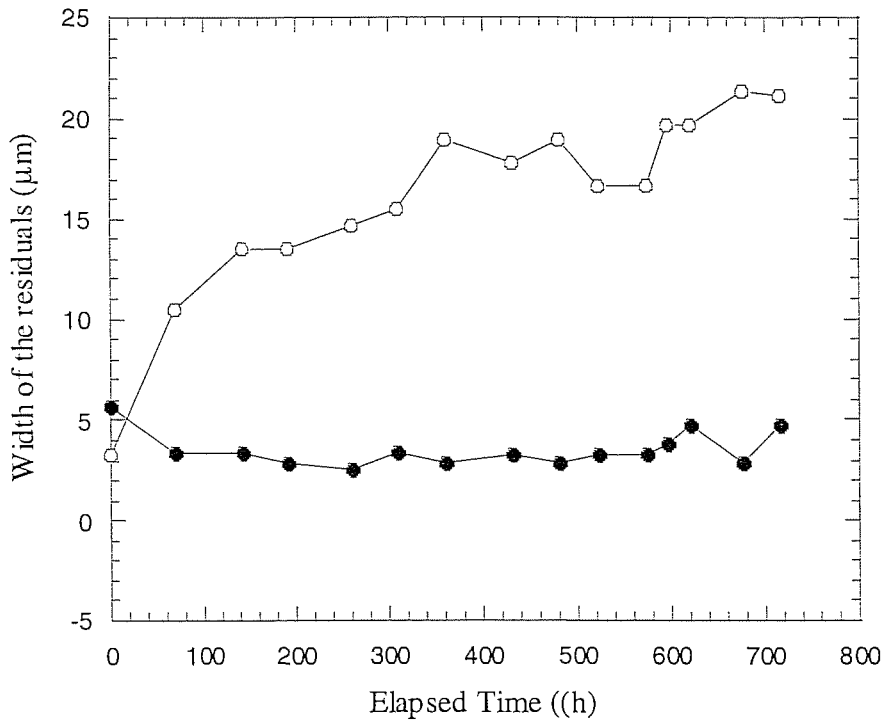
25
20
15
10
5
0
-5
Width of the residuals (μm)
0
100
200
300
400
500
600
700
800
Elapsed Time ((h)

Fig. 12

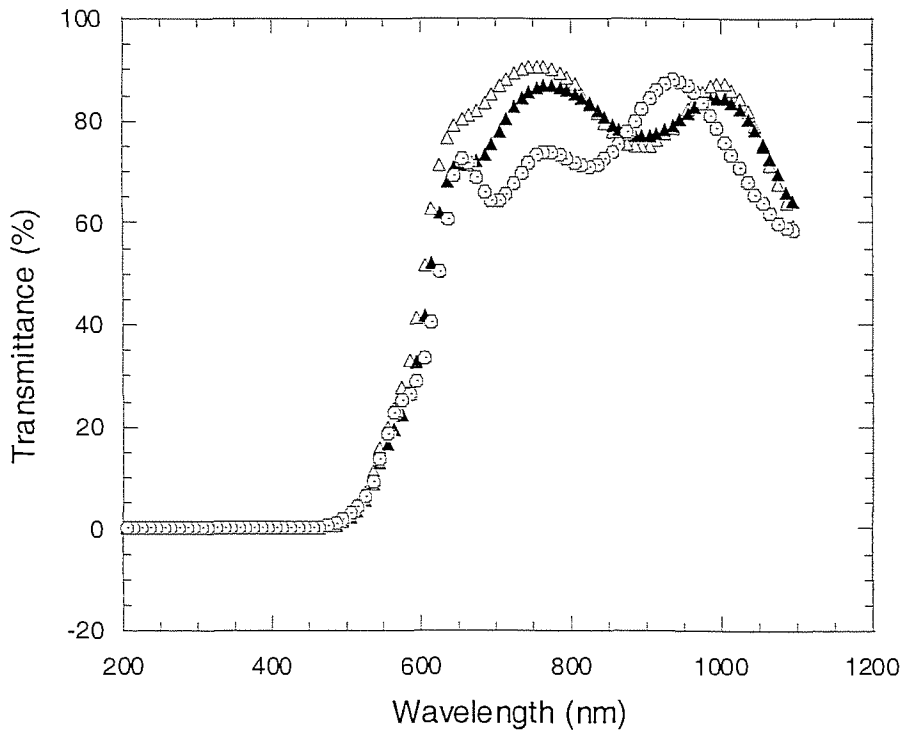
100
80
60
40
20
0
-20
Transmittance (%)
200
400
600
800
1000
1200
Wavelength (nm)

Fig. 13